

## Time Scales of the Greenland Freshwater Anomaly in the Subpolar North Atlantic

D. S. DUKHOVSKOY,<sup>a</sup> I. YASHAYAEV,<sup>b</sup> E. P. CHASSIGNET,<sup>a</sup> P. G. MYERS,<sup>c</sup> G. PLATOV,<sup>d</sup> AND A. PROSHUTINSKY<sup>e</sup>

<sup>a</sup>Center for Ocean–Atmospheric Prediction Studies, Florida State University, Tallahassee, Florida

<sup>b</sup>Bedford Institute of Oceanography, Fisheries and Oceans, Dartmouth, Nova Scotia, Canada

<sup>c</sup>Department of Earth and Atmospheric Sciences, University of Alberta, University of Alberta, Edmonton, Canada

<sup>d</sup>Institute of Computational Mathematics and Mathematical Geophysics, Novosibirsk, Russia

<sup>e</sup>Woods Hole Oceanographic Institution, Woods Hole, Massachusetts

(Manuscript received 31 July 2020, in final form 15 August 2021)

**ABSTRACT:** The impact of increasing Greenland freshwater discharge on the subpolar North Atlantic (SPNA) remains unknown as there are uncertainties associated with the time scales of the Greenland freshwater anomaly (GFWA) in the SPNA. Results from numerical simulations tracking GFWA and an analytical approach are employed to estimate the response time, suggesting that a decadal time scale (13 years) is required for the SPNA to adjust for increasing GFWA. Analytical solutions obtained for a long-lasting increase of freshwater discharge show a non-steady-state response of the SPNA with increasing content of the GFWA. In contrast, solutions for a short-lived pulse of freshwater demonstrate different responses of the SPNA with a rapid increase of freshwater in the domain followed by an exponential decay after the pulse has passed. The derived theoretical relation between time scales shows that residence time scales are time dependent for a non-steady-state case and asymptote the response time scale with time. The residence time of the GFWA deduced from Lagrangian experiments is close to and smaller than the response time, in agreement with the theory. The Lagrangian analysis shows dependence of the residence time on the entrance route of the GFWA and on the depth. The fraction of the GFWA exported through Davis Strait has limited impact on the interior basins, whereas the fraction entering the SPNA from the southwest Greenland shelf spreads into the interior regions. In both cases, the residence time of the GFWA increases with depth demonstrating long persistence of the freshwater anomaly in the subsurface layers.

**KEYWORDS:** North Atlantic Ocean; Lagrangian circulation/transport; Ocean circulation; Differential equations; Ocean models

### 1. Introduction

The subpolar North Atlantic (SPNA) is a key region for the Atlantic Ocean meridional circulation (AMOC) that plays important role in shaping regional and global climate (Stouffer et al. 2006; Trenberth and Fasullo 2017; Lozier et al. 2019). Therefore, the impact of accelerating Greenland Ice Sheet melting on the SPNA and AMOC has gained considerable attention (e.g., Bakker et al. 2016; Böning et al. 2016; Castelao et al. 2019). However, the extent and time scales of the SPNA response to the Greenland freshwater flux anomalies as well as the residence time of the Greenland freshwater are still unclear. This is particularly important for understanding the time-integrated effect of accelerated Greenland melting for the SPNA and global thermohaline circulation.

The SPNA encompasses the Labrador Sea, the Irminger Sea, and the Iceland Basin (Fig. 1a) dynamically linked by a large-scale cyclonic circulation formed by the North Atlantic Current and boundary currents (Fig. 1b). The boundary currents are the primary pathways of freshwater that convey low-salinity water from the Arctic Ocean and freshwater discharge from the Greenland Ice Sheet to the SPNA (e.g., Carmack et al. 2015; de Steur et al. 2018; Foukal et al. 2020). Since the 1960s, several negative salinity anomalies have propagated across the SPNA, impacting

thermohaline fields and convective processes in the region (Gelderloos et al. 2012; Yashayaev et al. 2015). The most remarkable of these events was the Great Salinity Anomaly (GSA) of the 1970s (Dickson et al. 1988), followed by two other freshening events in the 1980s and 1990s (Belkin et al. 1998; Belkin 2004).

Greenland freshwater discharge (hereafter simply Greenland discharge) was relatively steady from the 1950s until the early 1990s with an annual mean freshwater flux around 800–900 km<sup>3</sup> yr<sup>-1</sup>. In the early 1990s, the discharge started increasing (Bamber et al. 2012, 2018). Integrated over the time period from 1993 to 2016, surplus Greenland discharge from the Greenland Ice Sheet resulted in more than 5000 km<sup>3</sup> of freshwater anomaly [Greenland freshwater anomaly (GFWA)]. It is not known yet how the GFWA has impacted the SPNA. A strong freshening observed in the SPNA in the 2010s (Tesdal et al. 2018; Dukhovskoy et al. 2019; Holliday et al. 2020) could be a manifestation of the GFWA; however, the relationship between the freshening and the Greenland discharge is unclear. No other direct evidence of the GFWA has been found in hydrographic observations in the interior SPNA. Why is the impact of the GFWA on the SPNA not apparent unlike the GSA-type freshening events?

There are substantial differences between the GFWA and the decadal freshening events observed in the SPNA in terms of the time scales and the rate of freshwater influx. The previous freshening events originated from pulses of freshwater advected from the Arctic Ocean (Curry and Mauritzen 2005) whereas the GFWA, distributed over the

Corresponding author: Dmitry Dukhovskoy, ddukhovskoy@fsu.edu

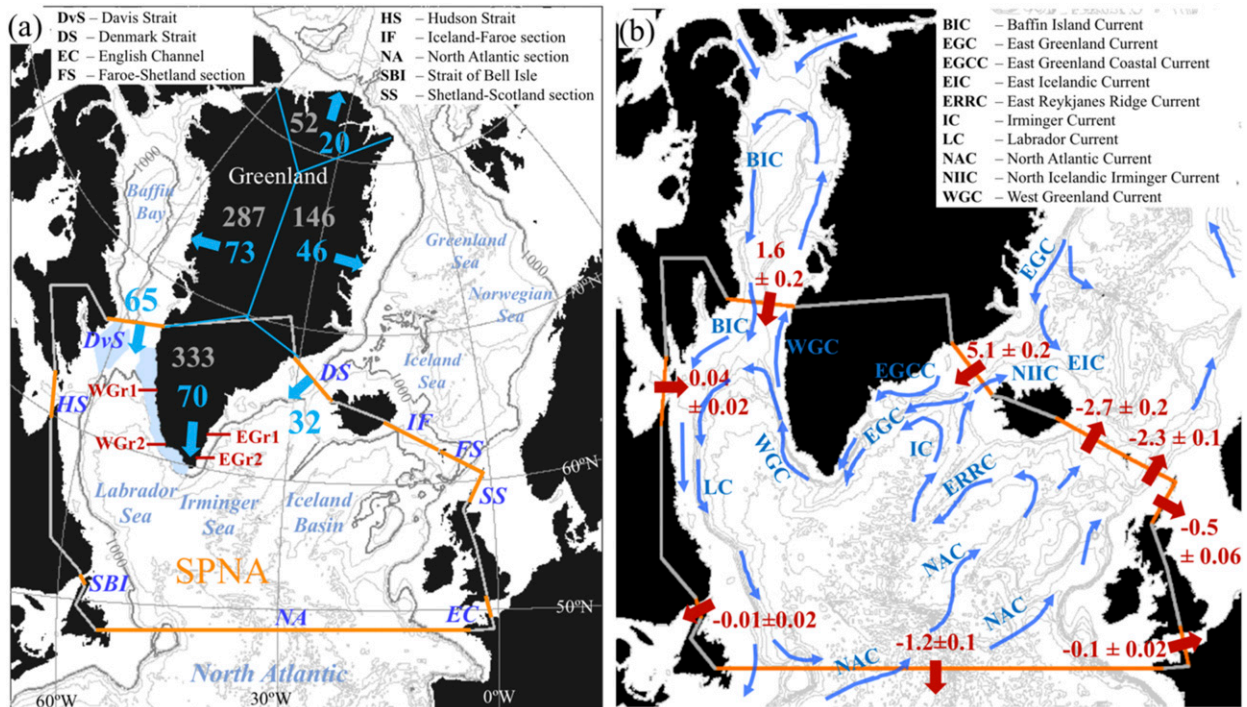


FIG. 1. Study domain. (a) The study domain includes the subpolar North Atlantic (bounded by the contour with orange segments indicating openings). The isobath contours are drawn every 1000 m up to the 1000-m isobath (dark gray) and the 500-m isobath. The blue arrows and numbers indicate annual mean fluxes of the GFWA through the Davis and Denmark Straits are estimated from the HYCOM model experiments with passive tracers tracking GFWA (Dukhovskoy et al. 2019). For Greenland, the mean annual freshwater fluxes (gray numbers) over 1958–92 and anomalies (blue) for 1993–2016 [deduced from the Greenland runoff dataset of Bamber et al. (2018)] are integrated for four regions (bounded by the blue lines). The light blue shaded areas over the eastern and northern Labrador shelves designate release locations of Lagrangian particles discussed in section 3a(1). The red lines on the south Greenland shelf designate locations of the sections shown in Fig. 5. (b) The blue arrows show mean circulation in the SPNA. Mean volume transports and their standard errors (Sv) derived from the HYCOM simulation are given for every opening along the SPNA boundary (the transports from the HYCOM simulation and from observations are summarized in Table 1).

extended Greenland coast, has been slowly (on average  $200\text{--}300\text{ km}^3\text{ yr}^{-1}$ ) released to the ocean since the early 1990s. The response of the SPNA to an abrupt release of freshwater (like the GSA) will likely be distinctly different from the response to a gradual release of surplus freshwater from Greenland. Hence, the question arises: How does the response of the SPNA to the GFWA differ from the response to the pulses of freshwater during the GSA-type events?

Given the relatively steady Greenland discharge before the 1990s, one can assume that the inflow, outflow, and volume of Greenland freshwater in the SPNA are in equilibrium for that period. Once the Greenland freshwater flux into the SPNA started to increase, that equilibrium was disturbed, and the system had to adjust. The time over which the system adjusts is characterized by a response time scale [see examples in Rodhe (1992) and Stouffer (2004)]. For the Greenland freshwater case, the response time scale will be the time over which the SPNA adjusts to the changing Greenland discharge and approaches an equilibrium between the inflow, outflow, and volume of the GFWA in the domain.

The response time scale of the SPNA is related to the residence time scales of the GFWA in the region. For a steady-state case and for systems that can be described as the first-order dynamical system the response time scale equals the residence times (Schwartz 1979; Bolin and Rodhe 1973). For a non-steady case, the relation between the residence time and response time scales is more complex.

The present study investigates the time scale over which the SPNA responds to the GFWA and residence time of the GFWA in the region. The response time scale of the SPNA to the GFWA is derived by employing a first-order dynamical system approximating a process of freshwater accumulation and release in the domain. The GFWA residence time scales are deduced from Lagrangian particle tracking using velocity fields from numerical experiments with passive tracer tracking of the GFWA introduced in Dukhovskoy et al. (2019).

In the following section, definitions and methodology are described, including the numerical passive tracer experiments, the dynamical system, and Lagrangian experiments. Response and residence time scales are derived in section 3. Section 4 investigates the relation between the response time and residence

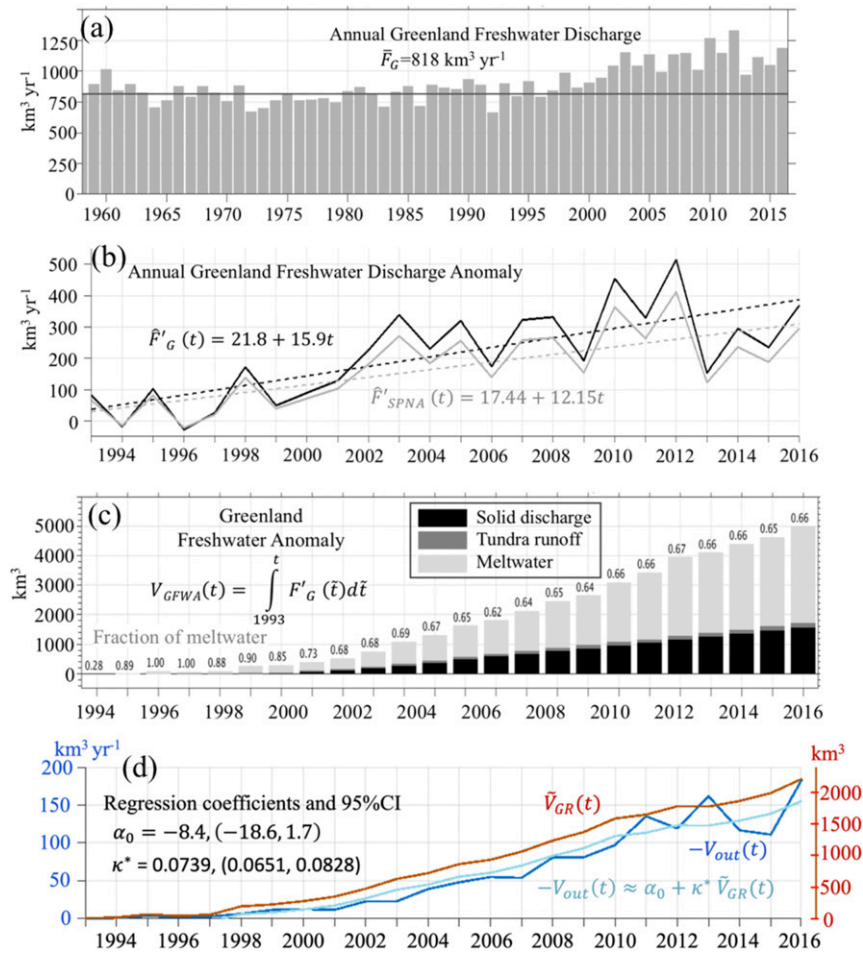


FIG. 2. Greenland freshwater mean and anomaly fluxes. (a) Annual total Greenland freshwater discharge ( $\text{km}^3 \text{yr}^{-1}$ ) derived from the monthly gridded product of Bamber et al. (2018). The horizontal solid line is the mean flux over 1958–93 ( $\bar{F}_G = 818.3 \text{ km}^3 \text{yr}^{-1}$ ) used as a reference for calculating the GFWA. (b) Annual Greenland freshwater flux anomaly ( $F'_G$ ). The gray solid curve is the fraction of the Greenland freshwater flux anomaly advected to the SPNA [section 2b(3)]. The dashed lines are corresponding linear trends. Time  $t$  is the number of years since 1993. (c) Time integration of the Greenland freshwater flux anomalies yields the GFWA. The diagram shows time series of the GFWA and its components (solid discharge, tundra runoff, and meltwater). The numbers indicate the fraction of meltwater in the GFWA. (d) Time series of the volume of the GFWA accumulated in the SPNA ( $\tilde{V}_{Gr}$ ) estimated from the HYCOM tracer numerical experiments (red; right vertical axis). The blue line shows the annual mean GFWA outflow (negated to ease the comparison with  $\tilde{V}_{Gr}$ ) from the SPNA derived from the HYCOM model simulation. The light blue line indicates the GFWA outflow (also negated) approximated by a linear regression. Estimates of the regression coefficients and their 95% confidence intervals (CIs) are listed in the diagram. Note that  $\alpha_0$  is insignificantly different from 0.

time scales. Section 5 discusses the response of the SPNA to a pulse of freshwater. The last two sections summarize and discuss the results.

## 2. Definitions and methodology

### a. Greenland freshwater anomaly

Estimates of Greenland discharge (1958–2016) are derived from a gridded product of Bamber et al. (2018).

Annual Greenland discharge can be expressed as the sum of a mean discharge ( $\bar{F}_G$ ) and an anomaly ( $F'_G$ ) (Figs. 2a and 2b):

$$F_G(t) = \bar{F}_G + F'_G(t). \quad (1)$$

The mean Greenland discharge and its standard error are computed for the 1958–1992 period and are  $818 \pm 13 \text{ km}^3 \text{yr}^{-1}$ . The Greenland discharge anomaly  $F'_G$  was increasing during 1993–2016 period (Fig. 2b), releasing on average  $209 \pm 30 \text{ km}^3$

TABLE 1. Mean volume fluxes (Sv) through sections and straits bounding the SPNA. Period of observations is in parentheses. Positive values represent a net flux into the SPNA

	Observation-based estimates	HYCOM-CICE
Davis Strait (DvS)	$1.6 \pm 0.5^a$ (2004–10)	$1.6 \pm 0.2$
Denmark Strait (DS)	$4.3 \pm 0.2^b$ (1994–2015)	$5.1 \pm 0.2$
Iceland–Faroe (IF)	$-3.4 \pm 0.6^b$ (1993–2015)	$-2.7 \pm 0.2$
Faroe–Shetland (FS)	$-0.5 \pm 0.6^b$ (2006–13)	$-2.3 \pm 0.1$
Shetland–Scotland (SS)	Combined SS and EC: $-0.6 \pm 0.6^b$ (1993–2015)	$-0.5 \pm 0.06$
English Channel (EC)		$-0.1 \pm 0.02$
North Atlantic (NA)		$-1.2 \pm 0.1$
Strait of Belle Isle (SBI)	$-0.13^c$ (Jul–Oct 1980)	$-0.01 \pm 0.02$
Hudson Strait (HS)	$0.11 \pm 0.24^d$ (Aug–Oct 1982)	$0.04 \pm 0.02$

<sup>a</sup> Curry et al. (2014).

<sup>b</sup> Østerhus et al. (2019).

<sup>c</sup> Petrie et al. (1988).

<sup>d</sup> Drinkwater (1988).

of additional freshwater per year. The increasing discharge can be approximated by a linear trend

$$F'_G(t) \approx \hat{F}'_G(t) = F_0 + pt, \quad (2)$$

where  $t$  is time (years since 1993),  $F_0 = 21.8 \text{ km}^3 \text{ yr}^{-1}$ , and the rate of change (increase) of the Greenland discharge  $p = 15.9 \text{ km}^3 \text{ yr}^{-2}$  (the 95% CI for  $p$  is [9.1, 21.3]; CI is confidence interval), which is similar to the estimate ( $16.9 \text{ km}^3 \text{ yr}^{-2}$ ) used by Böning et al. (2016).

The GFWA is defined as the time-integrated Greenland discharge anomaly from time  $t_0$  to  $t$  (Fig. 2c)

$$V_{\text{GFWA}}(t) = \int_{t_0}^t F'_G(\tilde{t}) d\tilde{t}. \quad (3)$$

In this study, the GFWA combines all components of the Greenland freshwater flux (Fig. 2c). However, the increase in ice sheet meltwater discharge has dominated the contributions from the solid and tundra runoff discharges since 1994 [~65% every year since 2000; Fig. 2c; note that a higher estimate of 84% since 2009 is reported in Enderlin et al. (2014)]. Integrated over the time period 1993–2016, the GFWA is  $5007 \pm 390 \text{ km}^3$ .

## b. Numerical experiments with Greenland passive tracers

### 1) DESCRIPTION OF THE HYCOM EXPERIMENTS

This study utilizes results from numerical experiments conducted within the Forum for Arctic Modeling and Observational Synthesis project (FAMOS; Proshutinsky et al. 2016). The analysis is based on tracer experiments performed with a coupled  $0.08^\circ$  Arctic Ocean Hybrid Coordinate Ocean Model (HYCOM) (Bleck 2002; Chassignet et al. 2003, 2006) and Los Alamos National Laboratory Sea Ice Code (CICE) version 4 (Hunke and Lipscomb 2010) (hereinafter referred to simply as HYCOM) configured for the North Atlantic, North Pacific, and Arctic Ocean and described in Dukhovskoy et al. (2019, hereinafter D2019). The HYCOM has a spatial resolution of  $\sim 4.5 \text{ km}$  in the study region. In these numerical experiments, the propagation and accumulation of the GFWA was tracked by a passive tracer that was continuously released along the coast of

Greenland at the freshwater sources. Locations and discharge rates of the Greenland freshwater sources were derived from the gridded product of Bamber et al. (2018). Simulated fields of tracer concentration were converted to concentrations of the GFWA in every grid cell of the computational domain (appendix A in D2019) to calculate the volume and transports of the freshwater anomaly in the SPNA.

Shown in Fig. 2d (red curve) is the HYCOM-based estimate of the GFWA retained in the SPNA at time  $t$  [ $\tilde{V}_{\text{GR}}(t)$ ] with the anomaly prescribed using the dataset of Bamber et al. (2018). By the end of 2016,  $2240 \text{ km}^3$  (~45%) of the GFWA were accumulated in the SPNA. This estimate will be used in the following analysis for the derivation of the time scales (section 3a).

### 2) SIMULATED AND OBSERVED VOLUME TRANSPORTS AND SURFACE CURRENTS

The HYCOM simulation shows a good agreement with observations in terms of ocean volume transports (Fig. 1b, Table 1) and surface circulation (Fig. 3). Time-average surface currents from HYCOM are compared against mean (2000–19) surface currents derived from trajectories of satellite-tracked surface drifting buoys (drifters) deployed within the NOAA Global Drifter Program. The trajectories were obtained from delayed-mode hourly data and real-time variable time-step data. The drifter data were temporally interpolated into 15-min time intervals, binned into hourly bins, and low-pass filtered to remove tidal and inertial oscillations. Then, the surface velocities were binned into a  $0.5^\circ$  grid. The simulated mesoscale surface circulation has close resemblance to the drifter-derived surface currents with well-defined large-scale cyclonic circulation in the SPNA, recirculation gyres, and strong eastward flow from the southern Labrador Sea. The magnitudes of the surface currents from the model and drifter-based estimates have alike positive-skewed distributions with similar statistics (Fig. 3).

### 3) FLUXES AND VERTICAL DISTRIBUTION OF THE GREENLAND FRESHWATER ANOMALY

The Greenland discharge flows into the Arctic Ocean and North Atlantic seas. Currents on the east Greenland shelf form a continuous pathway for Greenland freshwater (Fig. 1b),

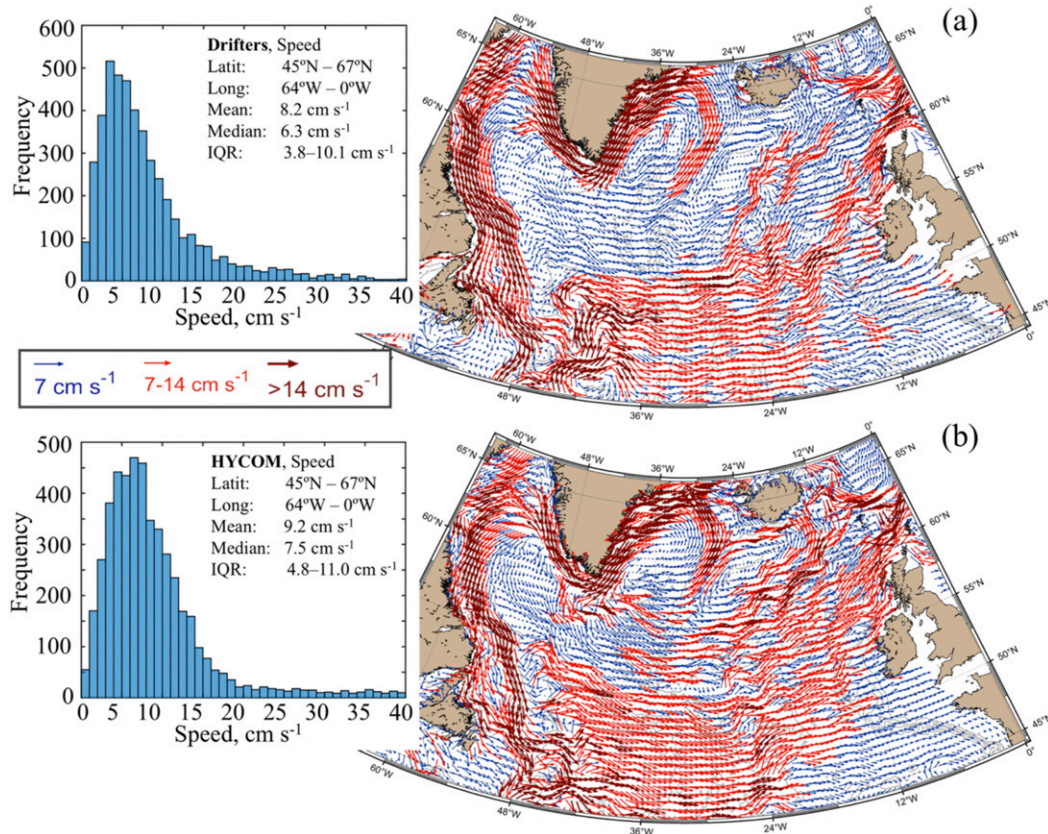


FIG. 3. Long-term mean surface currents, histograms, and statistics of the surface speed in the SPNA from surface drifters (a) and HYCOM (b). Time averaging period is 2000–19.

transporting it to the southwest Greenland shelf (Foukal et al. 2020). Advection of the GFWA fraction from the east shelf and local discharge results in high concentration of the GFWA on the southwest shelf [similar to Luo et al. (2016)] (Fig. 4), the region where the main outflow of the GFWA from the shelf occurs (Myers et al. 2009; D2019; Schulze Chretien and Frajka-Williams 2018). The boundary currents west of Greenland flow northward, carrying GFWA into Baffin Bay where the GFWA follows the large-scale cyclonic circulation and travels back toward Davis Strait after merging with the southward flowing Baffin Island Current. Here we quantify what proportion of the GFWA enters the SPNA using fluxes computed from the passive tracer fields in the HYCOM experiments of D2019.

There is a direct influx of the GFWA into the SPNA from the southern sector of Greenland and an indirect influx with the ocean boundary currents through the Davis and Denmark Straits (Fig. 1a). The direct flux of the GFWA into the SPNA averaged over 1993–2016 is around  $70 \pm 1.1 \text{ km}^3 \text{ yr}^{-1}$  (33%). The contribution of the Arctic Ocean sector to the surplus Greenland discharge is  $\sim 20 \pm 0.3 \text{ km}^3 \text{ yr}^{-1}$  (9.5%). The surplus discharge on the eastern shelf of Greenland is  $46 \pm 0.7 \text{ km}^3 \text{ yr}^{-1}$  (22%). On the east shelf, Greenland freshwater quickly propagates southward carried by the East Greenland Current and passes through Denmark Strait within a few months. The estimated net transport of the GFWA through Denmark

Strait is  $32 \pm 4 \text{ km}^3 \text{ yr}^{-1}$ . The average surplus Greenland discharge into Baffin Bay is  $73 \pm 1.1 \text{ km}^3 \text{ yr}^{-1}$  (35%). The model-based estimate of the GFWA net flux through Davis Strait is  $65 \pm 20 \text{ km}^3 \text{ yr}^{-1}$ . Thus, the modeled combined direct and indirect fluxes of the GFWA into the SPNA is  $167 \text{ km}^3 \text{ yr}^{-1}$  ( $\sim 0.8 F'_G$ ).

There is a notable discrepancy in vertical distribution of the GFWA in the Davis and Denmark Straits (Figs. 5a and 5b). In the central Davis Strait, the GFWA spreads down to 500–600 m. Therefore, the inflowing GFWA from Baffin Bay carried by the Baffin Island Current is mixed over the upper 500–600 m. In Denmark Strait, the GFWA is less mixed in the water column and is mostly confined to the top 200 m. The anomaly propagates southward with the East Greenland Coastal Current.

On its way to the southwest Greenland shelf, freshwater undergoes intense vertical mixing (Figs. 5c–f) driven by strong downwelling-favorable winds that dominate the southeast Greenland shelf (D2019). This result concurs with observational studies suggesting strong wind-driven vertical mixing of freshwater on the southeast Greenland shelf. Sutherland and Pickart (2008) found that the front of the East Greenland Coastal Current deepened and narrowed during downwelling winds. Håvik and Våge (2018) analyzed data from a mooring array deployed north of Denmark Strait on the Greenland shelf slope during 2011–12. In the time series of potential

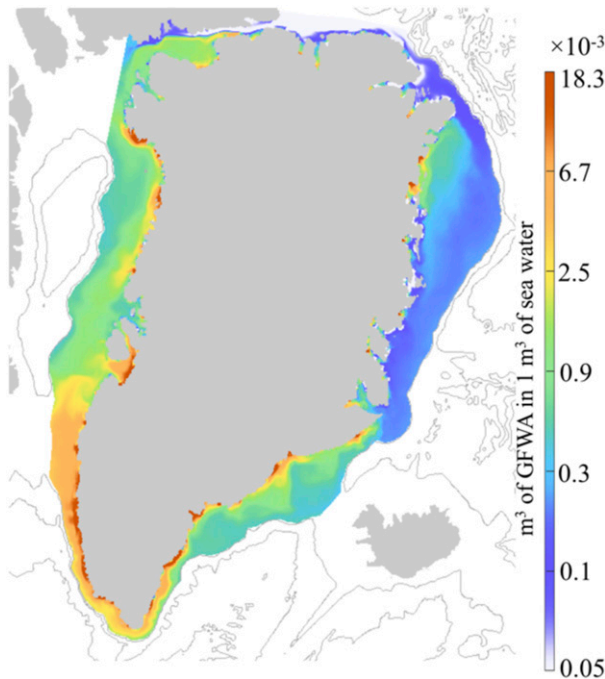


FIG. 4. Mean (2000–16) GFWA concentration in the upper 50 m on the Greenland shelf onshore of the 800-m isobath (the offshore concentration field is masked out) from the HYCOM simulation (D2019).

density at 550 m, the authors detected pulses of negative density anomalies that were related to the downwelling-favorable winds that enhanced vertical mixing of lighter water masses on the shelf.

### 3. Derivation of the time scales

#### a. Response time scale

##### 1) ANALYTICAL MODEL

A simple approach can be used to estimate the response time of a system or the residence time of some quantity in a control volume whose mass changes in time as a function of input, output, and sink–source functions (e.g., Miller and McPherson 1991; Schlosser et al. 1994). The SPNA can be considered as a control volume with a source (inflow of the GFWA) and a sink (outflow of the GFWA) along the boundaries (the contour line in Fig. 1). It is further assumed that the export of the GFWA is proportional to the volume of the GFWA in the SPNA (a first-order approximation). This approximation is valid for our considered case as demonstrated by Fig. 2d. The diagram shows a strong relation between the outflow of the GFWA [negated,  $-V_{\text{out}}(t)$ ] and the volume of the GFWA in the SPNA derived from the HYCOM experiments ( $\tilde{V}_{\text{GR}}$ ). The light-blue line depicts export of the GFWA out of the SPNA approximated with a simple linear relation:

$$-V_{\text{out}}(t) \approx \alpha_0 + k \tilde{V}_{\text{GR}}(t). \quad (4)$$

Note that the coefficient  $\alpha_0$  is not significantly different from 0. Therefore, it is still accurate to approximate the export as  $-V_{\text{out}}(t) \approx k \tilde{V}_{\text{GR}}(t)$ ; that is, the export is proportional to the volume of the GFWA in the SPNA (the light blue curve in Fig. 2d).

The following first-order autonomous dynamical system is used to describe time-evolving changes in the system caused by a change in external conditions (e.g., Skogestad 2009; Teschl 2012):

$$\frac{dV(t)}{dt} + kV(t) - F(t) = 0, \quad (5)$$

$$V(t_0) = V_0, \quad (6)$$

where  $V(t)$  is dependent variable (volume of freshwater anomaly in the domain at time  $t$ ),  $t_0$  is initial time, and  $k = \tau^{-1}$ , where  $\tau$  is the response time scale that needs to be estimated for the SPNA. In some studies, coefficient  $k$  is referred to as the removal coefficient as it characterizes the rate of removal of material from the domain (e.g., Schwartz 1979). For a steady-state case,  $k$  determines how fast the system approaches the new steady state. The model [Eq. (5)] with initial condition [Eq. (6)] describes the change in freshwater volume of the SPNA caused by accumulated GFWA [ $V(t)$ ].

##### 2) RESPONSE TIME SCALE FROM THE ANALYTICAL MODEL

The general solution of [Eq. (5)] with the initial condition [Eq. (6)] is determined by the forcing function  $F(t)$ . Forcing represented with a Heaviside step function, results in a steady-state solution. Here,  $F(t)$  is a linearly increasing function given by [Eq. (2)] resulting in a non-steady-state solution. The forcing function approximates the fraction of the surplus Greenland discharge that corresponds to the 1993–2016 value (section 2a), fluxed into the SPNA.

Following the analysis in section 2b(3), a fraction (0.8) of the Greenland discharge anomaly advected to the SPNA is considered (gray curve in Fig. 2b). In this case, regression parameters [Eq. (2)] are  $F_0 = 17.44 \text{ km}^3 \text{ yr}^{-1}$  and the rate of change of the Greenland discharge  $p = 12.15 \text{ km}^3 \text{ yr}^{-2}$  (the 95% CI for  $p$  is [7.3, 17.0]). The general solution of [Eq. (5)] with  $F(t) = \hat{F}'_G(t)$  given by [Eq. (2)] and with the initial condition [Eq. (6)] is

$$V(t) = \frac{F_0}{k} + \frac{p}{k^2}(kt - 1) + \left( V_0 + \frac{p}{k^2} - \frac{F_0}{k} \right) e^{-kt}. \quad (7)$$

The solution [Eq. (7)] shows that the GFWA volume accumulated in the SPNA does not reach a steady state but continues to grow, driven by the linearly increasing Greenland discharge. Equation (7) is solved iteratively for  $k$  with  $V = \tilde{V}_{\text{GR}}(t = 24) = 2240 \text{ km}^3$  (Fig. 2d). The derived estimate is  $k \approx 1/13 \text{ yr}^{-1}$  and the time scale  $\tau$  is  $\sim 13$  years (Fig. 6).

Alternatively, the response time scale  $\tau$  can be deduced directly from the export of the GFWA out of the SPNA ( $V_{\text{out}}$ ) using the assumption  $-V_{\text{out}}(t) = kV(t)$ , as discussed in section 3a(1). Following this approach,  $k$  is 0.0739

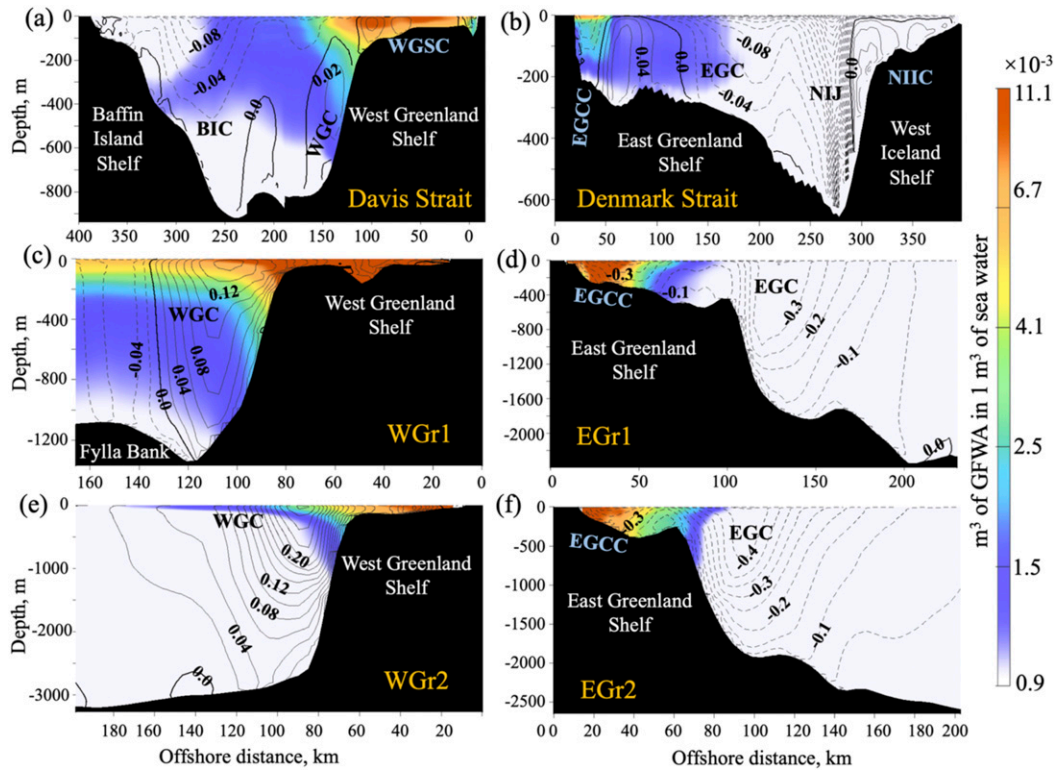


FIG. 5. Concentration of the GFWA from the HYCOM simulation with passive tracers in the last model year (2016). The concentration is given in  $\text{m}^3$  of the GFWA in  $1 \text{ m}^3$  of seawater ( $1 \times 10^{-3} \text{ m}^3 = 1 \text{ L}$ ). Vertical distribution of the GFWA in the (a) Davis and (b) Denmark Straits and along sections on the (c),(e) western and (d),(f) eastern Greenland shelf. The sections are shown in Fig. 1a. Note the different depth ranges. Major currents are listed in the figures (NIJ = North Iceland Jet; WGSC = West Greenland Shelf Current; the other notations are given in Fig. 1b).

(Fig. 2d), which corresponds to  $\tau \approx 13.5$  years (the 95% CI is [12.1, 15.4]). The estimate agrees well with the estimate  $\tau \approx 13$  years derived by iteration of the analytical solution [Eq. (7)], demonstrating that both approaches provide similar response time scales for the SPNA.

b. Residence time scales

1) EXPERIMENTS WITH LAGRANGIAN PARTICLES

The residence time scale of the GFWA is evaluated by performing Lagrangian experiments using velocity fields from the HYCOM experiment (D2019) extended for 3 years to cover a longer time period. The GFWA is discretized with 3600 Lagrangian particles that are randomly seeded on the southwest Greenland shelf and northern Labrador Sea shelf (the light-blue shaded areas in Fig. 1a) and advected by the daily mean HYCOM velocity fields using explicit four-stage Runge–Kutta method with a 2-day time stepping. Release sites shown in Fig. 1a represent two major entrance locations of the GFWA into the SPNA. The one on the northern Labrador Sea shelf represents the fraction of the GFWA exported from Baffin Bay. The other location on the southwest Greenland shelf corresponds to the region of high concentration of the GFWA (Fig. 4). Most of the Greenland freshwater (>80%; D2019) leaves the

shelf at this location (Schulze Chretien and Frajka-Williams 2018; Castelao et al. 2019).

The HYCOM experiments with passive tracers showed vertical mixing of the GFWA on the Greenland shelf and offshore (Fig. 5). Observational studies also provide evidence of vertical mixing of the Greenland freshwater on the shelf and

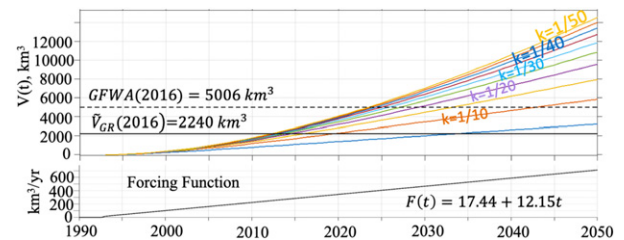


FIG. 6. Solutions for [Eq. (5)] with  $V_0 = 0$  showing progress of GFWA accumulation in the SPNA for the linearly increasing discharge rate anomaly [Eq. (2)] for different  $k$ . The forcing is shown in the bottom subpanel. The dashed line is the GFWA by the end of 2016 ( $5006 \text{ km}^3$ ). The black solid line is the fraction of the GFWA in the SPNA by the end of 2016 estimated from the HYCOM tracer experiments (the red line in Fig. 2d). The curve with  $k = 1/13 \text{ yr}^{-1}$  intersecting the black solid line at 2016 is the solution to the problem.

TABLE 2. Characteristics of the HYCOM layers used for the Lagrangian experiments. The depths of the HYCOM layers are average values over the SPNA deeper than 500 m.

HYCOM characteristics	Depth groups of Lagrangian particles			
	Group 1	Group 2	Group 2	Group 4
Layer number	10	15	23	29
Target densities, $\sigma_{2000}$ ( $\text{kg m}^{-3}$ )	26.00	30.65	35.20	36.52
Mean layer depth (m)	48	88	153	480
Mean depth of the top layer interface (m)	44	84	149	434
Mean depth of the bottom layer interface (m)	52	92	159	528

interior Labrador and Irminger Seas. For example, helium and neon profiles in the SPNA revealed the highest concentration of Greenland glacial water in the upper 400 m (Rhein et al. 2018). In the layers below 400 m, the glacial water was homogeneously distributed over the water column down to 2000 m.

To track propagation of the GFWA at different depths, the particles are seeded by four groups in different model layers from the near-surface (group 1) to deeper layers (groups 2–4) at each release location. Average depths and other characteristics of the HYCOM layers in the deep ocean for each group are listed in Table 2. Note that the shown depths do not represent the release depths of the particles over the shelf (which are shallower) but rather the average depth at which the particles are advected in the deep ocean.

## 2) RESIDENCE TIME SCALE FROM THE LAGRANGIAN EXPERIMENTS

The residence time ( $\tau_r$ ) of a water mass or a set of water parcels in a control volume  $\Omega$  can be defined in terms of three time quantities (Bolin and Rodhe 1973): the turnover time ( $\tau_{to}$ ), mean age ( $\tau_{ma}$ ), and mean transit ( $\tau_{mt}$ ) time. Turnover time is the ratio of the volume of the water mass (here, GFWA) to the inflow rate or outflow rate. Mean age is the average age of parcels in  $\Omega$ . Mean transit time is the average age of water parcels leaving  $\Omega$ . The residence time of the GFWA is obtained from the statistics of the Lagrangian particles. The section starts with the description of pathways of the GFWA derived from the Lagrangian experiments followed by analysis of the residence times.

There are several common features in the pathways of the Lagrangian particles released on the southwest Greenland shelf and on the northern Labrador Sea shelf (Figs. 7 and 8). First, the particles from all groups start moving cyclonically along the Labrador Sea shelf carried by the Labrador Current (over the shelf) and the shelf-break branch of the West Greenland Current toward Newfoundland. At the Great Banks of Newfoundland, some fraction of the particles continues northeast with the North Atlantic Current. On their way, the particles leave the shelf, spreading into the interior SPNA.

Second, there is a depth dependence of the particles' pathways. During the first year, particles in the deeper layers from groups 3 and 4 (advected at 150 and 450 m) travel along the Labrador Sea continental shelf slope following the  $f/h$  contours. The particles from these groups have higher

occurrence probability in the deep southwest Labrador Sea and in the central and eastern interior SPNA (Fig. 9). By contrast, the particles in the near-surface layer (group 1) stay more onshore (Figs. 7a and 7e). Both for the Labrador shelf and Greenland shelf release locations, particles in the near-surface layer have more frequent presence on the shelves especially near Newfoundland (Fig. 9).

Third, about half of the particles advected in the upper 50 m (group 1) leave the SPNA during the first 1–3 years, whereas the particles from the other groups leave the domain at a notably slower rate (4–11 years), especially those advected at 450 m (Fig. 8).

Last, after  $\sim 10$  years, the presence of the particles on the shelf is notably reduced. By that time, the particles retained in the domain are predominantly in the interior SPNA inside the 1000-m isobath (Fig. 8).

The main difference between the Greenland shelf particles and the Labrador Sea shelf particles is their presence in the interior SPNA and on the western Labrador Sea shelf. During the first year, the Labrador shelf particles from depth groups 1–3 travel predominantly inshore advected by the Labrador Current and by the end of the year the particles are concentrated over the western Labrador Sea shelf and continental slope (Figs. 7e–g and 9e–g), whereas the Greenland shelf particles from the same groups stay offshore, carried by the shelf-break branch of the West Greenland Current (Figs. 7a–c and 9a–c). The Greenland shelf particles are more dispersed over the interior Labrador Sea.

Next, after reaching the Grand Banks of Newfoundland,  $\sim 35\%$  of the Labrador shelf particles in the near-surface layer (group 1) continue south with the Labrador Current leaving the SPNA. By contrast, a smaller fraction of the Greenland shelf particles ( $<20\%$ ) leaves the SPNA. The experiments show that the number of particles from the northern Labrador Sea shelf in the interior SPNA is substantially lower than the number of Greenland shelf particles during all years at all depths (Figs. 8 and 9). Finally, the northern Labrador Sea shelf particles from group 4 ( $\sim 450$  m) follow the continental slope of the western Labrador Sea shelf and spread into the southern Labrador Sea (Figs. 7h and 9h). Conversely, the Greenland shelf particles spread over the whole interior Labrador Sea basin (Figs. 7d and 9d).

Derived distributions of the age of the particles ( $\tau_{age}$ ) provide estimates for the residence time scale of the GFWA in the SPNA, suggesting two main conclusions. First, the residence



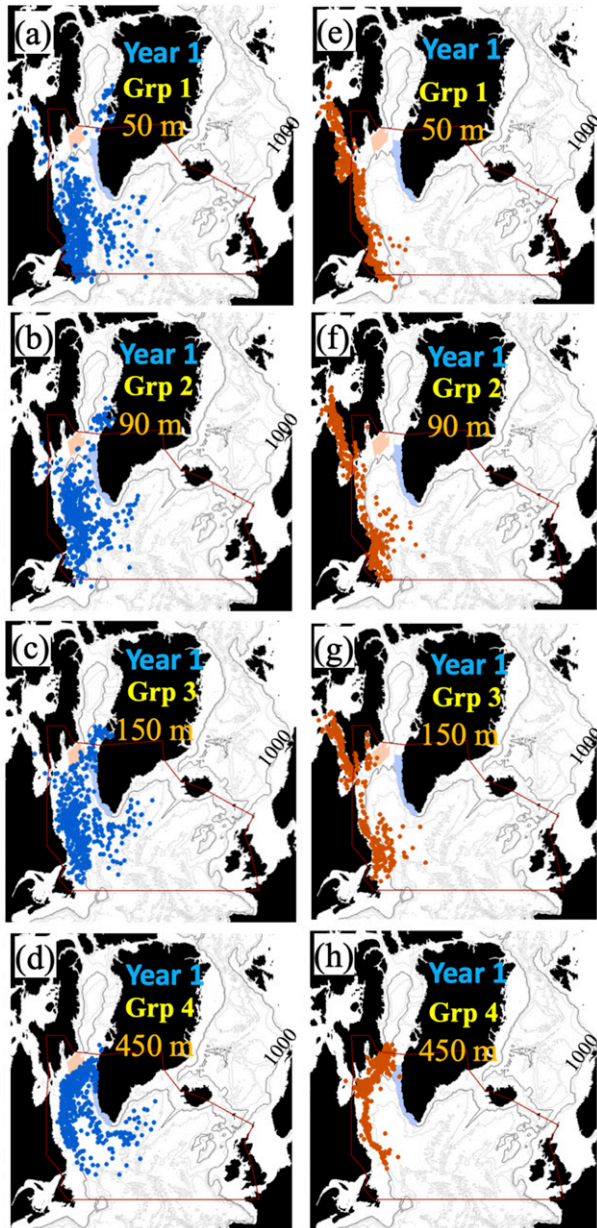


FIG. 7. Location of the Lagrangian particles by the end of the first year. The red and blue shadings designate two release locations. (a)–(d) Particles released on the southwest Greenland shelf for depth groups 1–4. (e)–(h) Particles released on the northern Labrador Sea shelf for depth groups 1–4 (in rows) depict particles released at different HYCOM vertical layers (Table 2). The numbers indicate nominal depths for each group. The shown depths are approximate depths of layers in the deep (>800 m) ocean where particles from each group circulate. Note these depths do not represent the release depths on the shelves. The red bounding line designates the SPNA domain. The gray contours are isobaths drawn every 1000 m. The dark gray contour is the 1000-m isobath.

time of the GFWA fluxed from Baffin Bay is shorter than that of the GFWA from the southwest Greenland shelf, especially for the depth groups 1 and 2 advected in the upper layers (Figs. 10a and 10b). This is apparent from the differences in the cumulative distribution functions and exceedance of the particles' age ( $\tau_{\text{age}}$ ). For example, the 0.8 probability that  $\tau_{\text{age}} \leq 1$  corresponds to  $t = 1$  year for the Labrador shelf particles and  $t = 8$  years for the Greenland shelf particles in the upper 50 m (Fig. 10a). The distributions of  $\tau_{\text{age}}$  for particles at the deepest layer (group 4) are closer for the Greenland and Labrador shelf particles, but still distinctly different (Fig. 10d).

Second, the residence time is depth-dependent. The particles advected in the near-surface layer (50 m) tend to leave the SPNA during the first 1–3 years (Figs. 10a). The distributions for groups 3 and 4 are flatter (Figs. 10c and 10d), indicating that the particles in the deeper layers stay significantly longer in the SPNA than the particles in the near-surface depths. The result is more evident in the boxplot diagrams of the particles' ages (Fig. 11a). For both release locations, there is an obvious increase of the particles' age (and hence residence time) in the SPNA with depth. Estimated mean ages ( $\tau_{\text{ma}}$ ) for the particle groups and the 95% CIs of the means show significantly (statistically) different mean ages both across the depth groups and within the depth groups for different release locations (Fig. 11b).

Therefore, the Lagrangian experiments suggest that residence time of the GFWA in the SPNA depends on the entrance route of the GFWA and depths at which the anomaly circulates in the domain. For the GFWA fluxed into the SPNA from Baffin Bay, the mean residence time increases from 1.2 years for 50-m circulation depth to 10.1 years for 450 m. For the GFWA entering the SPNA via the southwest Greenland shelf, the mean residence time increases from 4.4 years (50 m) to 13.3 years (450 m).

#### 4. Analysis

In the previous section, response ( $\tau$ ) and residence ( $\tau_r$ ) time scales for the GFWA have been derived. The two terms are related but not necessarily identical, especially for a non-steady case. This complicates direct comparison of the time scales. In the following sections, an analytical relationship between the time scales is derived and the time scales are compared.

##### a. Relation between time scales for a non-steady-state case

For a steady-state process that can be described as the first-order dynamical system [section 3a(1)] the response time ( $\tau$ ) may be interpreted as any of the residence time scales ( $\tau_{\text{to}}$ ,  $\tau_{\text{ma}}$ , or  $\tau_{\text{mt}}$ ) because all the residence times are equal to the  $k^{-1}$  (Schwartz 1979; Bolin and Rodhe 1973). For the linearly increasing discharge anomaly, the relationship between  $\tau$  and  $\tau_r$  is more complex because the solution is non-steady state.

The following relations are derived for our case based on Schwartz (1979), who established a relationship among different residence times for non-steady-state conditions. Schwartz introduced the persistence function  $A(t, t_0)$  to evaluate the time scales and described it as the rate at which material is introduced in the volume at time  $t_0$  remaining at time  $t$ . For our case, the persistence function is

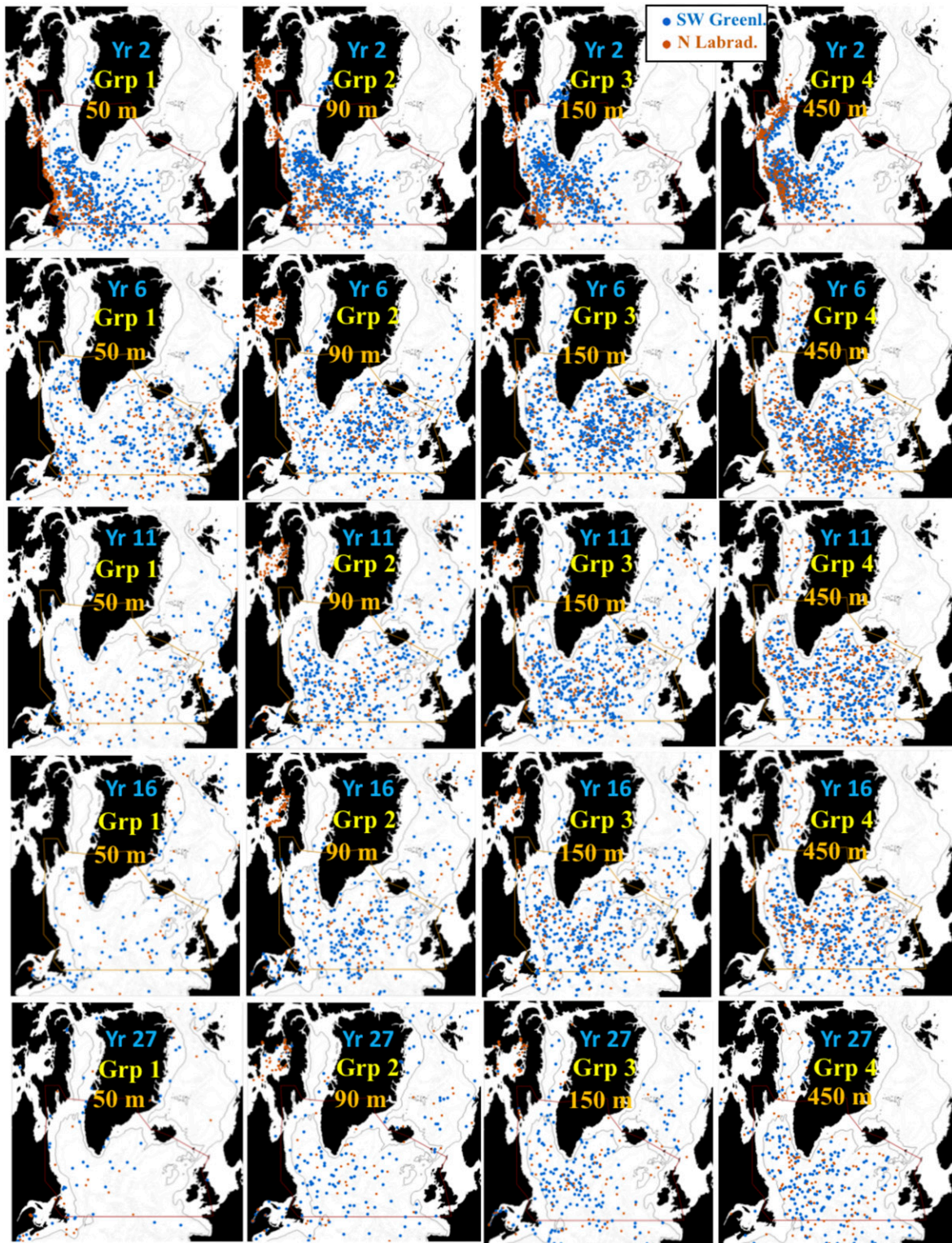


FIG. 8. Particles' positions at the end of selected years. Particles released on the southwest Greenland shelf (blue dots) and northern Labrador Sea shelf (red dots) are shown together. The particles' depth groups are in columns, the years are in rows. The red bounding line designates the SPNA domain. The dark gray contour is the 1000-m isobath.

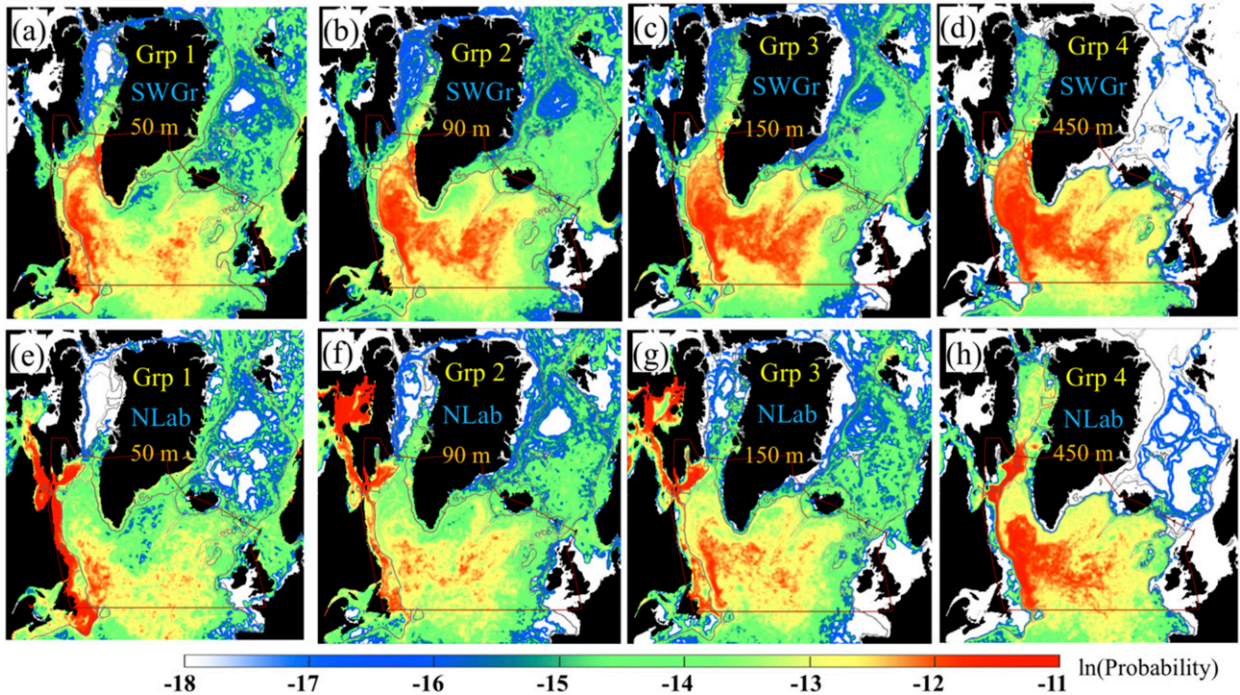


FIG. 9. Probability maps of observing a particle in a grid cell at any given day during the time of integration (1993–2019) for particles released (top) on the southwest Greenland shelf and (bottom) on the northern Labrador Sea shelf. In columns are probabilities for the particles advected at (a),(e) 50, (b),(f) 90, (c),(g) 150, and (d),(h) 450 m. The colors designate the probabilities on a natural logarithmic scale. Integrated over the model domain, the probability is 1. The bounding red contour denotes the SPNA region.

$$A(t, t_0) \equiv F(t_0)e^{-k(t-t_0)}; \quad (8)$$

that is, the flux of the GFWA introduced into the SPNA at time  $t_0$  remaining at time  $t$ . The term  $F(t_0) \equiv \hat{F}'_G(t_0) = F_0 + pt_0$  is the linearly increasing forcing function [Eq. (2)].

Following Schwartz (1979), the volume of the GFWA present in the SPNA at time  $t$  is

$$V(t) = \int_0^t F(t_0)e^{-k(t-t_0)} dt_0. \quad (9)$$

It is straightforward to show that after integration [Eq. (9)] becomes

$$V(t) = \frac{F_0}{k} + \frac{p}{k^2}(kt - 1) + \left(\frac{p}{k^2} - \frac{F_0}{k}\right)e^{-kt}, \quad (10)$$

which equals the analytical solution [Eq. (7)] obtained for the linear increasing GFWA with initial condition  $V_0 = 0$ , as expected.

For a non-steady-state case, the turnover time is not uniquely defined because the inflow and outflow of the GFWA are not equal. Hence, there are two possible definitions of  $\tau_{to}$  [Eqs. (11) and (12)] relating the amount of water mass present in  $\Omega$  at time  $t$  to the inflow and outflow rates, respectively:

$$\tau_{to}^{(1)}(t) = \frac{V(t)}{F(t)}, \quad (11)$$

$$\tau_{to}^{(2)}(t) = \frac{V(t)}{kV(t)} = k^{-1} = \tau. \quad (12)$$

Note that, in general, the time scales are time-dependent and are not identical. The second definition equals the response time scale from the analytical solution. The turnover time scale  $\tau_{to}^{(1)}$  is shown in Fig. 12 for  $V(t)$  given by [Eq. (7)] and  $k = 1/13 \text{ yr}^{-1}$  [derived for the GFWA in section 3a(2)]. The time scale converges to  $k^{-1} = 13$  years, which is the response time scale. Therefore, for the analyzed system, the response time scale derived from the analytical model [Eq. (5)] provides an estimate for the turnover time of the GFWA fluxed into the SPNA at a linearly increasing rate.

For the dynamical system [Eq. (5)], the mean transit time is equal to the mean age (Schwartz 1979), meaning that the average time GFWA spends in the SPNA equals the mean transit time for the GFWA. The mean age of the GFWA present in the domain for the non-steady solution is

$$\tau_{ma}(t) = \frac{1}{V(t)} \int_0^t (t - t_0)F(t_0)e^{-k(t-t_0)} dt_0. \quad (13)$$

Again, for a non-steady case, mean age is time dependent and increases with time. As time progresses, the fraction of the GFWA that is mixed into the deeper layers grows, increasing  $\bar{\tau}_{ma}$ , as predicted by [Eq. (13)]. It can be shown, however, that  $\lim_{t \rightarrow \infty} \tau_{ma}(t) \rightarrow k^{-1}$ . From [Eq. (13)]

$$\lim_{t \rightarrow \infty} \tau_{ma}(t) = \lim_{t \rightarrow \infty} \left[ \frac{1}{V(t)} \int_0^t (t - t_0)(F_0 + pt_0)e^{-k(t-t_0)} dt_0 \right]. \quad (14)$$

After integration and noting that  $\lim_{t \rightarrow \infty} e^{-kt} \rightarrow 0$ , [Eq. (14)] becomes

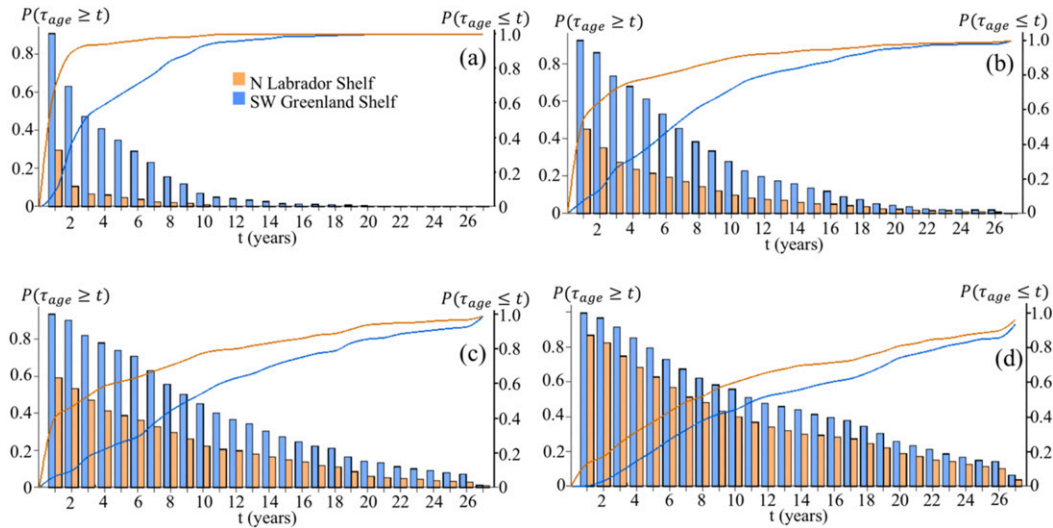


FIG. 10. Cumulative distribution functions and exceedance of a particle age for the particle groups advected at (a) 50, (b) 90, (c) 150, and (d) 450 m. The lines are the cumulative distribution functions (right axis) showing the probability that the age or transit time of a particle is at most  $t$  years [ $P(\tau_{\text{ma}} \leq t) = \int_{-\infty}^t f(\bar{t}) d\bar{t}$ , where  $f(t)$  is the probability density function]. The bar diagrams (left axis) show exceedance, i.e., the probability that the age or transit time of a particle is at least  $t$  years [ $P(\tau_{\text{ma}} \geq t) = 1 - P(t)$ ]. The scale is on the left axis. The colors designate release locations of the Lagrangian particles.

$$\lim_{t \rightarrow \infty} \tau_{\text{ma}}(t) = \lim_{t \rightarrow \infty} \left\{ \frac{1}{V(t)k^2} \left[ \left( F_0 + pt - \frac{p}{k} \right) - \frac{p}{k} \right] \right\}. \quad (15)$$

Using the analytical solution [Eq. (7)] for  $V(t)$  with  $V^0 = 0$  and noting that

$$\lim_{t \rightarrow \infty} V(t) \approx \lim_{t \rightarrow \infty} \frac{1}{k} \left( F_0 + pt - \frac{p}{k} \right), \quad (16)$$

the following is derived:

$$\lim_{t \rightarrow \infty} \tau_{\text{ma}}(t) = \lim_{t \rightarrow \infty} \left\{ \frac{1}{k^2} \left[ \frac{1}{k} \left( F_0 + pt - \frac{p}{k} \right) \right]^{-1} \times \left[ \left( F_0 + pt - \frac{p}{k} \right) - \frac{p}{k} \right] \right\} \rightarrow \frac{1}{k}. \quad (17)$$

Therefore, the mean age converges to  $k^{-1} = 13$  yr as  $t \rightarrow \infty$  as shown in Fig. 12. Hence, the analytically derived response time scale is an estimate for the limits of the mean age of the GFWA for the non-steady-state solution as  $t \rightarrow \infty$ . For  $t \ll \infty$ ,  $\tau_{\text{ma}}(t) < k^{-1}$ ; that is, during the first several decades, the mean age of the GFWA is smaller than the analytically derived response time scale. For example, after 26 years the mean age of the GFWA in the SPNA is around 7 years, according to [Eq. (13)].

Increasing residence time scales (Fig. 12) are due to the redistribution of the GFWA in the water column by vertical mixing. As freshwater is mixed downward (below 100–150 m), it enters the layers with longer residence times than the surface layers, increasing the overall residence time of the GFWA in the domain.

#### b. Comparison of the time scales from the analytical solution and Lagrangian experiments

The time scales deduced from the Lagrangian experiments characterize the residence time of the GFWA within the ocean layers where they circulated, whereas the analytically derived response time scale  $\tau$  describes accumulation of the GFWA integrated over the whole depth. Therefore, the residence time scales derived from the Lagrangian analysis need to be depth-averaged for comparison with the response time scale and with the theory in section 4a. Depth-averaged time scales of the Labrador shelf particles and the Greenland shelf particles are weighted proportionally to the fluxes of the GFWA through Davis Strait and from the southwest Greenland Shelf (Fig. 1a), that is,

$$\bar{\tau}_{\text{ma}} = 0.39 \bar{\tau}_{\text{ma}}^{(L)} + 0.61 \bar{\tau}_{\text{ma}}^{(G)}, \quad (18)$$

where  $\bar{\tau}_{\text{ma}}$  is the depth-averaged mean age, and  $\bar{\tau}_{\text{ma}}^{(L)} = D^{-1} \int_{-D}^0 \tau_{\text{ma}}^{(L)}(z) dz$  is depth-averaged mean age of the Labrador particles; similarly  $\bar{\tau}_{\text{ma}}^{(G)}$  is the depth-averaged mean age of the Greenland shelf particles, and  $D$  is depth. The choice of the lower limit of integration ( $D$ ) depends on the vertical spreading of the GFWA. Previous observational and modeling studies suggest that traceable Greenland freshwater remains predominantly in the upper 1000 m in the interior SPNA (e.g., Rhein et al. 2018; Fig. 9 in D2019). The following estimates of the depth-averaged mean age and their 95% CI (in the parentheses) are derived: for  $D = 500$  m,  $\bar{\tau}_{\text{ma}} = 9.1$  (8.5, 9.7) yr; for  $D = 800$  m,  $\bar{\tau}_{\text{ma}} = 10.3$  (9.6, 10.9) yr; for  $D = 1000$  m,  $\bar{\tau}_{\text{ma}} = 10.6$  (9.9, 11.3) yr.

Therefore, depth-averaged mean age (9–11 years) is close to  $\tau$  (13 years) and  $\bar{\tau}_{\text{ma}} < \tau$ , as expected [Eq. (13)], yet slightly bigger than theoretical  $\bar{\tau}_{\text{ma}}$  after 26 years ( $\sim 7$  years). This

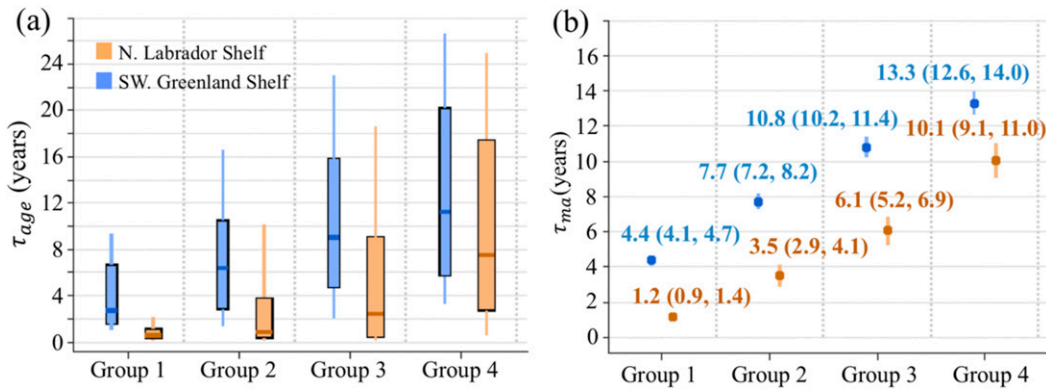


FIG. 11. Statistics of the particles' age for the particle depth groups. The colors indicate particles released at the southwest Greenland shelf (blue) and northern Labrador Sea shelf (orange). (a) Boxplot diagrams of particle ages. The box shows the interquartile range. The line in the box is the median. The whiskers indicate the interdecile range. (b) Mean age estimates ( $\tau_{ma}$ ). Listed are the means and their 95% CIs.

stems from the assumption that the GFWA is homogeneously mixed over  $D$  when depth averaging has been performed. In reality, GFWA is nonuniformly distributed in the water column and the vertical distribution is space dependent. A more accurate depth-dependent distribution of the Lagrangian particles would provide  $\bar{\tau}_{ma}$  that is in a better agreement with the theoretical value.

### 5. Response of the SPNA to a pulse of freshwater

To compare the SPNA response to a GSA-type freshening event, an analytical solution is obtained for an abrupt pulse of freshwater approximating large negative salinity anomalies advected into the SPNA during the freshening events. We argue that the response of the SPNA to a pulse of freshwater can be approximated using the same system [Eq. (5)], as long as the anomaly is advected from external sources and is not produced inside the SPNA. Here, the forcing function is represented as a bump function

$$F(t) = \Phi [u(t - a) - u(t - b)], \quad (19)$$

where  $u(t)$  is the Heaviside step function, so that  $t = a$  is time when the forcing is abruptly turned on and  $t = b$  is time when

the forcing is turned off. Using Laplace transform of Eqs. (5) and (19) and taking  $V_0 = 0$ , the solution for Eq. (5) is found as

$$V(t) = \frac{\Phi}{k} \left[ u(t - a)(1 - e^{-k(t-a)}) - u(t - b)(1 - e^{-k(t-b)}) \right]. \quad (20)$$

The width of the bump ( $\Delta t = b - a$ ) represents the duration of the freshwater pulse. In the limit ( $\Delta t \rightarrow 0$ ), the forcing becomes a delta function. Having analyzed historical hydrographic data, Curry and Mauritzen (2005) concluded that the GSA was associated with an additional freshwater export of  $\sim 2000 \text{ km}^3 \text{ yr}^{-1}$  from the Arctic Ocean for 5 years at the end of the 1960s. Following Curry and Mauritzen (2005),  $\Delta t = 5$  and  $\Phi = 2000 \text{ km}^3 \text{ yr}^{-1}$

The solution of the problem with the bump forcing function (Fig. 13) is qualitatively different from the solution for the linearly increasing GFWA (Fig. 6). In this case, the SPNA rapidly accumulates freshwater anomaly during the period of the increased freshwater flux. After the forcing  $F(t)$  is turned off ( $t \geq t_b$ ), the solution [Eq. (20)] describes the rate of removal of freshwater anomaly from the system. For the freshwater bump case, the response time scale characterizes the time that it takes to reduce the volume of the accumulated water mass to  $e^{-1}$  of its maximum at

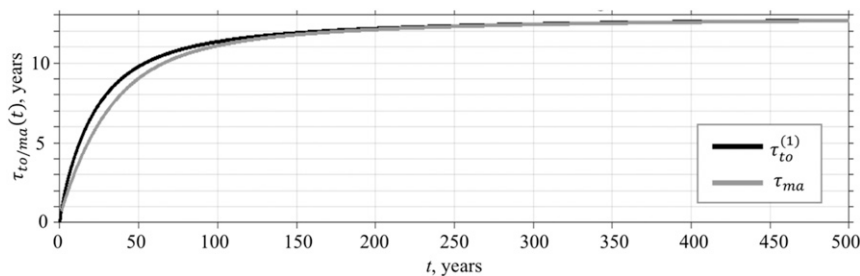


FIG. 12. Turnover time [Eq. (12)] and mean age [Eq. (13)] of the GFWA for the linearly increasing flux of the GFWA into the SPNA. The time scales converge to the response time scale  $\tau = 13$  years obtained from [Eq. (7)].

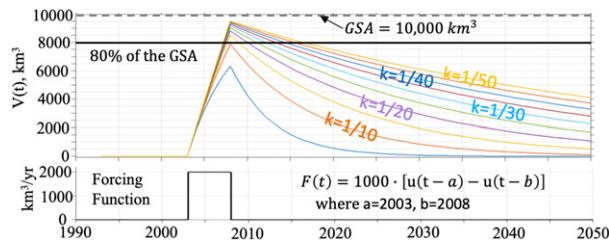


FIG. 13. Solutions for Eq. (5) with  $V_0 = 0$  showing progress of a freshwater anomaly accumulation in the SPNA for the bump forcing function [Eq. (19)] for different  $k$ . The forcing is shown in the bottom subpanel. The dashed line shows the volume of freshwater in the GSA used as the total input into the SPNA in this solution. The total volume of the GSA ( $10\,000\text{ km}^3$ ) equals time-integrated value of the forcing function shown in the bottom subpanel. The black solid line indicates the 80% of the freshwater volume accumulated in the SPNA used to determine  $k$  ( $11\text{ yr}^{-1}$ ).

$t_b$  ( $e$ -folding time). Also  $\tau$  determines the peak value of the freshwater anomaly in the SPNA.

The response time scale ( $\tau$ ) for this case can be estimated based on Curry and Mauritzen (2005), who stated that  $\sim 80\%$  of the anomalous freshening during the 1960s to 1990s ended up in the SPNA (referred to as “Subpolar Basins” in their study). Note that this is a higher estimate than for the GFWA fraction ( $\sim 45\%$ ) retained in the SPNA (Fig. 2d). The solution corresponding to  $\max[V(t)] = 8000\text{ km}^3$  is the one with  $k = 1/11\text{ yr}^{-1}$ , which is close to  $k = 1/13\text{ yr}^{-1}$  derived for the GFWA.

## 6. Discussion

### a. Derived time scales

The analytically derived response time scale of the SPNA to the GFWA (13 years) is close to the decadal time scale of oceanic variability in the SPNA shown by previous studies (e.g., Chafik et al. 2016; Reverdin et al. 1997). Weaver et al. (1991) showed that freshwater forcing imposed at the ocean surface excites decadal and interdecadal variations in the North Atlantic thermohaline circulation, arguing that these scales are intrinsic time scales of oceanic variability in the region. Multidecadal time scales characterizing the response of the North Atlantic thermohaline circulation to surface freshwater fluxes were reported by Sévellec et al. (2009). The results of our study indicate that the SPNA adjusts quickly (13 years) to surplus Greenland discharge of the magnitude considered here. The quick response is explained by the slow rate of freshwater anomalies fluxed into the region. At this influx rate, the surplus freshwater does not impact the large-scale circulation in the SPNA and presumably has a minor impact on thermohaline circulation (e.g., Hu et al. 2009; Swingedouw et al. 2015) as those take a much longer time to adjust (Stouffer 2004; Sévellec et al. 2009).

Sensitivity of the SPNA thermohaline circulation to Greenland melting remains however unknown. Previous modeling studies suggest that an additional discharge of Greenland freshwater at a rate greater than  $\sim 0.1\text{ Sv}$  ( $1\text{ Sv} \equiv 10^6\text{ m}^3\text{ s}^{-1}$ ) (present observed rate is  $\sim 0.01\text{ Sv}$ ) would impact the thermohaline circulation

weakening or shutting down AMOC (Stouffer et al. 2006; Swingedouw et al. 2007; Hu et al. 2009). Therefore, for the magnitudes of the freshwater anomaly analyzed in the paper, the response time scale ( $\tau$ ) is mainly determined by the residence time of the GFWA in the SPNA.

There are uncertainties, however, involved in the derivation of the time scales. The estimates rely on the HYCOM simulation of the Greenland freshwater spreading, mixing, and circulation in the SPNA. While the mesoscale circulation and oceanic fluxes are well represented in the HYCOM simulations, the accuracy of diapycnal mixing of the freshwater anomaly in the model is hard to evaluate. Using different mixing schemes can clearly change the amount of the GFWA accumulated in the SPNA and, as a result, impact the response time scale estimates. Depending on spatial resolution, numerical schemes, turbulence parameterization, and spurious diapycnal mixing, other numerical models may provide estimates of the GFWA fluxes and its accumulation in the SPNA that are different from HYCOM. This might result in different estimates of the time scales; nevertheless, we conjecture that the estimates should be comparable with those presented here, at least for the models of comparable spatial resolution, vertical mixing schemes, and low spurious diapycnal mixing. The HYCOM-based estimate of the volume of GFWA accumulated in the SPNA by the end of 2016 was compared with other simulations participating in the Greenland tracer experiment [not presented here but discussed in Dukhovskoy et al. (2016)]. The estimates agreed within  $\sim 20\%$ , providing the lower and upper bounds of the estimate between 11 and 23 years (assuming same GFWA influxes).

Another source of uncertainty is the fraction of the GFWA fluxed into the SPNA through the Davis and Denmark Straits (Fig. 1a). Again, the estimates were derived from the HYCOM simulation and there is uncertainty involved in these estimates owing to a relatively short length of the simulation and increasing Greenland discharge (i.e., the mean is not stationary). The largest uncertainty is related to the flux estimate through Davis Strait where the GFWA flux has strong seasonality and interannual variability. However, the derived time response estimate is only weakly sensitive to the uncertainties in the influx of the GFWA. For example, assuming that the total volume of the anomalous Greenland discharge is fluxed into the SPNA (the mean is  $209\text{ km}^3\text{ yr}^{-1}$ ) the response time scale is 11.3 years, which is still close to 13 years estimated for  $167\text{ km}^3\text{ yr}^{-1}$ .

### b. GFWA entrance routes

The Lagrangian experiments demonstrate distinctly different pathways and residence time scales for the fraction of the GFWA fluxed into the SPNA through Davis Strait (northern Labrador Sea shelf) and the fraction entering from the southwest Greenland shelf (Figs. 8–12). These results concur with model tracer studies by Myers (2005), who showed that freshwater from Baffin Bay did not enter the interior Labrador Sea, whereas freshwater from the south Greenland shelf did propagate into the central Labrador Sea. Therefore, we conjecture that the GFWA exported from Baffin Bay has a small impact on the interior SPNA except for the fraction in the deeper

subsurface layers, which spreads into the interior southern and central Labrador Sea and central SPNA (Fig. 10k). Thus, it could be argued that the Greenland freshwater traveling from the southwest Greenland shelf is the main contributor to the GFWA that spreads to the interior SPNA and circulates there for a decade, which is consistent with other studies (Luo et al. 2016; Castelao et al. 2019).

### c. GFWA and freshening events in the SPNA

Analytical solutions for the dynamical system [Eq. (5)] clearly illustrate different responses of the SPNA to either a pulse of freshwater or a slowly increasing Greenland discharge. The results presented here suggest different evolutions of the freshwater anomaly and associated freshening in the SPNA originated from the GFWA and freshwater pulses propagating from the Arctic Ocean (through either Fram Strait or Davis Strait). The GFWA is fluxed into the SPNA at a slow rate and unevenly distributed over the coast of Greenland. This surplus freshwater does not have a strong impact on the water column stability because it is mixed into the deeper layers by wind-driven mixing on the Greenland shelf (Sutherland and Pickart 2008; Håvik and Våge 2018; D2019) and by deep convection in the interior SPNA (Yashayaev and Loder 2016, 2017; de Jong et al. 2018). We therefore infer that a substantial fraction of the GFWA propagates into subsurface layers below 100 m where it can circulate within the SPNA for about 10–15 years, whereas the GFWA fraction in the near-surface layers (above 100 m) is quickly (in less than 7 years) removed from the SPNA by the surface currents. Therefore, most of the GFWA accumulated in the SPNA circulates below 100 m, while the surface salinity remains largely unaffected on a multiyear time scale. Thus, the overall impact of the GFWA on surface salinity in the SPNA is expected to be small (as stated in D2019) and the presence of the GFWA cannot be easily tracked from salinity surface observations.

In the case of freshwater pulses, the flux of freshwater anomaly transported into the SPNA is about 10 times larger than the surplus Greenland freshwater flux, resulting in quick accumulation of freshwater anomaly in the SPNA (Fig. 13). Although we argue that general response of the SPNA to short-lived freshening events is well approximated by the analytical model, the estimated response time scale ( $\tau$ ) should be taken with reservation. Hindcast numerical experiments of the GSA-type events with passive tracers tracking the anomaly would provide necessary information on pathways and accumulation of freshwater anomaly in the SPNA. Also, freshwater volume in the GSA-type events might need to be reassessed given the ambiguity associated with the choice of reference salinity in the calculation of freshwater content reported in the previous studies (Schauer and Losch 2019).

Due to the large volume of surplus freshwater advected into the SPNA over a short period of time, the freshwater anomaly substantially shifts surface salinity, increasing water column stability and inhibiting vertical mixing and spreading of freshwater into the subsurface layers (leading to positive salinity anomalies in the subsurface Labrador Sea; e.g., Yashayaev et al. 2015). Unlike the GFWA, this freshwater

anomaly predominantly stays in the near-surface layers, causing strong freshening in the SPNA. This idea concurs with paleoclimate studies suggesting that abrupt climate change events were likely caused by pulses of meltwater from the ice sheets of North America impacting AMOC (e.g., Rahmstorf 2002).

With regard to the 2010s freshening in the SPNA, the direct relation to the GFWA is unlikely. Observed freshening with magnitudes 0.1–0.3 developed during 3–5 years and primarily in the upper 200 m (D2019; Holliday et al. 2020), which is more characteristic of a freshwater pulse propagating into the SPNA (Dickson et al. 1988). However, the GFWA could have contributed to the overall freshwater content anomaly in the SPNA, since the upper 1000 m of the SPNA acquired about 6600 km<sup>3</sup> of freshwater anomaly [again, the reported estimate depends on the choice of the reference salinity and represents a fraction of freshwater in contrast to the GFWA that is pure freshwater according to Schauer and Losch (2019)] during 2012–16 (Holliday et al. 2020). Deep propagation and a wide spreading of the freshening in the SPNA could be attributed to the accumulated GFWA in the subsurface layers.

## 7. Conclusions

The study shows that the SPNA response to the perturbation in the Greenland freshwater discharge has decadal time scale ( $\tau = 13$  yr). The response time scale is mainly determined by the residence time of the GFWA in the SPNA. For the non-steady case, the residence time scales are not constant and approach  $\tau$  in the limit as  $t \rightarrow \infty$ . The residence time of the GFWA derived from the Lagrangian experiments is 9–11 years, which is close to and smaller than  $\tau$ , in agreement with the theory (section 4a). The SPNA response to the GFWA is qualitatively different from the response to the GSA-type events characterized by strong freshening due to quick (a few years) accumulation of surplus freshwater in the region. In contrast, accelerating Greenland melt results in a slow but still growing volume of freshwater anomaly in the SPNA. Therefore, the role of the surplus Greenland freshwater in the SPNA in the future depends on whether the melting continues to grow or levels off. A slowdown of the freshwater discharge anomaly from the Greenland Ice Sheet occurred during 2012–16 (Figs. 2a and 2b). Recent satellite data revealed an unprecedented summer mass loss of the Greenland Ice Sheet in 2019 (Velicogna et al. 2020), which may indicate the return of an accelerating Greenland discharge, meaning that volume of the GFWA in the SPNA will continue to grow. Presently, the impact of the GFWA remains mainly inconspicuous in the interior SPNA, but the long-term increase of the freshwater content in the SPNA will likely have a profound impact on thermohaline circulation in the subpolar regions and the Arctic Ocean, potentially leading to a weaker AMOC, lower ocean fluxes through the Canadian Arctic Archipelago, and reduced volume transport through Bering Strait into the Arctic Ocean (Hu et al. 2009, 2010; Hu and Myers 2014; Jackson and Wood 2018).

*Acknowledgments.* D. S. Dukhovskoy and E. P. Chassignet were funded by the DOE (Award DE-SC0014378) and HYCOM NOPP (Award N00014-19-1-2674). The HYCOM-CICE simulations were supported by a grant of computer time

from the DoD High-Performance Computing Modernization Program at NRL SSC. G. Platov was funded by the RSF N19-17-00154. P. G. Myers was funded by an NSERC Discovery Grant (Grant RGPIN 04357). A. Proshutinsky was funded by FAMOS project (NSF Grant NSF 14-584). The authors thank the anonymous reviewers for valuable and helpful comments, and Ilya Dukhovskoy and Eva Dukhovskaya for proofreading the manuscript.

**Data availability statement.** The daily mean fields from the 0.08 AO HYCOM experiment with the passive tracer are available at the HYCOM data server ([ftp://ftp.hycom.org/datasets/ARCC0.08/expt\\_11.0/data/](ftp://ftp.hycom.org/datasets/ARCC0.08/expt_11.0/data/)). Surface drifter data were obtained from processed delayed mode hourly data ([https://www.aoml.noaa.gov/phod/gdp/hourly\\_data.php](https://www.aoml.noaa.gov/phod/gdp/hourly_data.php)) and real-time variable-time-step data ([https://www.aoml.noaa.gov/phod/gdp/real-time\\_data.php](https://www.aoml.noaa.gov/phod/gdp/real-time_data.php)).

#### REFERENCES

- Bakker, P., and Coauthors, 2016: Fate of the Atlantic Meridional Overturning Circulation: Strong decline under continued warming and Greenland melting. *Geophys. Res. Lett.*, **43**, 12 252–12 260, <https://doi.org/10.1002/2016GL070457>.
- Bamber, J., M. van den Broeke, J. Ettema, J. Lenaerts, and E. Rignot, 2012: Recent large increases in freshwater fluxes from Greenland into the North Atlantic. *Geophys. Res. Lett.*, **39**, L19501, <https://doi.org/10.1029/2012GL052552>.
- , A. J. Tedstone, M. D. King, I. M. Howat, E. M. Enderlin, M. R. van den Broeke, and B. Noel, 2018: Land ice freshwater budget of the Arctic and North Atlantic Oceans: 1. Data, methods, and results. *J. Geophys. Res. Oceans*, **123**, 1827–1837, <https://doi.org/10.1002/2017JC013605>.
- Belkin, I. M., 2004: Propagation of the “Great Salinity Anomaly” of the 1990s around the northern North Atlantic. *Geophys. Res. Lett.*, **31**, L08306, <https://doi.org/10.1029/2003GL019334>.
- , S. Levitus, J. Antonov, and S.-A. Malmberg, 1998: “Great Salinity Anomalies” in the North Atlantic. *Prog. Oceanogr.*, **41** (1), 1–68, [https://doi.org/10.1016/S0079-6611\(98\)00015-9](https://doi.org/10.1016/S0079-6611(98)00015-9).
- Bleck, R., 2002: An oceanic general circulation model framed in hybrid isopycnic-Cartesian coordinates. *Ocean Modell.*, **37**, 55–88, [https://doi.org/10.1016/S1463-5003\(01\)00012-9](https://doi.org/10.1016/S1463-5003(01)00012-9).
- Bolin, B., and H. Rodhe, 1973: A note on the concepts of age distribution and transit time in natural reservoirs. *Tellus*, **25**, 58–62, <https://doi.org/10.3402/tellusa.v25i1.9644>.
- Böning, C. W., M. Scheinert, J. Dengg, A. Biastoch, and A. Funk, 2016: Decadal variability of subpolar gyre transport and its reverberation in the North Atlantic overturning. *Geophys. Res. Lett.*, **33**, L21S01, <https://doi.org/10.1029/2006GL026906>.
- Carmack, E., P. Winsor, and W. Williams, 2015: The contiguous pan-arctic Riverine Coastal Domain: A unifying concept. *Prog. Oceanogr.*, **139**, 13–23, <https://doi.org/10.1016/j.pocean.2015.07.014>.
- Castelao, R. M., and Coauthors, 2019: Controls on the transport of meltwater from the southern Greenland ice sheet in the Labrador Sea. *J. Geophys. Res. Oceans*, **124**, 3551–3560, <https://doi.org/10.1029/2019JC015159>.
- Chafik, L., S. Häkkinen, M. H. England, J. A. Carton, S. Nigam, A. Ruiz-Barradas, A. Hannachi, and L. Miller, 2016: Global linkages originating from decadal oceanic variability in the subpolar North Atlantic. *Geophys. Res. Lett.*, **43**, 10 909–10 919, <https://doi.org/10.1002/2016GL071134>.
- Chassignet, E. P., L. T. Smith, G. R. Halliwell, and R. Bleck, 2003: North Atlantic simulations with the HYbrid Coordinate Ocean Model (HYCOM): Impact of the vertical coordinate choice, reference density, and thermobaricity. *J. Phys. Oceanogr.*, **33**, 2504–2526, [https://doi.org/10.1175/1520-0485\(2003\)033<2504:NASWTH>2.0.CO;2](https://doi.org/10.1175/1520-0485(2003)033<2504:NASWTH>2.0.CO;2).
- , and Coauthors, 2006: Generalized vertical coordinates for eddy-resolving global and coastal ocean forecasts. *Oceanography*, **19**, 20–31, <https://doi.org/10.5670/oceanog.2006.95>.
- Curry, B., C. M. Lee, B. Petrie, R. E. Moritz, and R. Kwok, 2014: Multiyear volume, liquid freshwater, and sea ice transports through Davis Strait, 2004–10. *J. Phys. Oceanogr.*, **44**, 1244–1266, <https://doi.org/10.1175/JPO-D-13-0177.1>.
- Curry, R., and C. Mauritzen, 2005: Dilution of the northern North Atlantic Ocean in recent decades. *Science*, **308**, 1772–1774, <https://doi.org/10.1126/science.1109477>.
- de Jong, M. F., M. Oltmanns, J. Karstensen, and L. de Steur, 2018: Deep convection in the Irminger Sea observed with a dense mooring array. *Oceanography*, **31**, 50–59, <https://doi.org/10.5670/oceanog.2018.109>.
- de Steur, L., C. Peralta-Ferriz, and O. Pavlova, 2018: Freshwater export in the East Greenland Current freshens the North Atlantic. *Geophys. Res. Lett.*, **45**, 13 359–13 366, <https://doi.org/10.1029/2018GL080207>.
- Dickson, R. R., J. Meincke, S. Malmberg, and A. J. Lee, 1988: The “Great Salinity Anomaly” in the northern North Atlantic 1968–1982. *Prog. Oceanogr.*, **20**, 103–151, [https://doi.org/10.1016/0079-6611\(88\)90049-3](https://doi.org/10.1016/0079-6611(88)90049-3).
- Drinkwater, K. F., 1988: On the mean and tidal currents in Hudson Strait. *Atmos.–Ocean*, **26**, 252266, <https://doi.org/10.1080/07055900.1988.9649302>.
- Dukhovskoy, D. S., and Coauthors, 2016: Greenland freshwater pathways in the sub-Arctic Seas from model experiments with passive tracers. *J. Geophys. Res. Oceans*, **121**, 877–907, <https://doi.org/10.1002/2015JC011290>.
- , I. Yashayaev, A. Proshutinsky, J. L. Bamber, I. L. Bashmachnikov, E. P. Chassignet, C. M. Lee, and A. J. Tedstone, 2019: Role of Greenland freshwater anomaly in the recent freshening of the subpolar North Atlantic. *J. Geophys. Res. Oceans*, **124**, 3333–3360, <https://doi.org/10.1029/2018JC014686>.
- Enderlin, E. M., I. M. Howat, S. Jeong, M.-J. Noh, J. H. van Angelen, and M. R. van den Broeke, 2014: An improved mass budget for the Greenland ice sheet. *Geophys. Res. Lett.*, **41**, 866–872, <https://doi.org/10.1002/2013GL059010>.
- Foukal, N. P., R. Gelderloos, and R. Pickart, 2020: A continuous pathway for fresh water along the East Greenland shelf. *Sci. Adv.*, **6**, eabc4254, <https://doi.org/10.1126/sciadv.abc4254>.
- Gelderloos, R., F. Straneo, and C. A. Katsman, 2012: Mechanisms behind the temporary shutdown of deep convection in the Labrador Sea: Lessons from the Great Salinity Anomaly years 1968–71. *J. Climate*, **25**, 6743–6755, <https://doi.org/10.1175/JCLI-D-11-00549.1>.
- Håvik, L., and K. Våge, 2018: Wind-driven coastal upwelling and downwelling in the shelf break East Greenland Current. *J. Geophys. Res. Oceans*, **123**, 6106–6115, <https://doi.org/10.1029/2018JC014273>.
- Holliday, N. P., 2020: Ocean circulation causes the largest freshening event for 120 years in eastern subpolar North Atlantic. *Nat. Commun.*, **11**, 585, <https://doi.org/10.1038/s41467-020-14474-y>.
- Hu, A., G. A. Meehl, W. Han, and J. Yin, 2009: Transient response of the MOC and climate to potential melting of the Greenland Ice Sheet in the 21st century. *Geophys. Res. Lett.*, **36**, L10707, <https://doi.org/10.1029/2009GL037998>.



- , and Coauthors, 2010: Influence of Bering Strait flow and North Atlantic circulation on glacial sea level changes. *Nat. Geosci.*, **3**, 118–121, <https://doi.org/10.1038/ngeo729>.
- Hu, X., and P. G. Myers, 2014: Changes to the Canadian Arctic Archipelago sea ice and freshwater fluxes in the twenty-first century under the Intergovernmental Panel on Climate Change A1B climate scenario. *Atmos.–Ocean*, **52**, 331–350, <https://doi.org/10.1080/07055900.2014.942592>.
- Hunke, E. C., and W. H. Lipscomb, 2010: CICE: The Los Alamos Sea Ice Model documentation and software user's manual, version 4.1. LA-CC-06-012, 76 pp.
- Jackson, L. C., and R. A. Wood, 2018: Timescales of AMOC decline in response to fresh water forcing. *Climate Dyn.*, **51**, 1333–1350, <https://doi.org/10.1007/s00382-017-3957-6>.
- Lozier, M. S., and Coauthors, 2019: A sea change in our view of overturning in the subpolar North Atlantic. *Science*, **363**, 516–521, <https://doi.org/10.1126/science.aau6592>.
- Luo, H., R. Castelao, A. K. Rennermalm, M. Tedesco, A. Bracco, P. L. Yager, and T. L. Mote, 2016: Oceanic transport of surface meltwater from the southern Greenland ice sheet. *Nat. Geosci.*, **9**, 528–532, <https://doi.org/10.1038/ngeo2708>.
- Miller, R. L., and B. F. McPherson, 1991: Estimating estuarine flushing and residence times in Charlotte Harbor, Florida, via salt balance and a box model. *Limnol. Oceanogr.*, **36**, 602–612, <https://doi.org/10.4319/lo.1991.36.3.0602>.
- Myers, P. G., 2005: Impact of freshwater from the Canadian Arctic Archipelago on Labrador Sea Water formation. *Geophys. Res. Lett.*, **32**, L06605, <https://doi.org/10.1029/2004GL022082>.
- , C. Donnelly, and M. H. Ribergaard, 2009: Structure and variability of the West Greenland Current in summer derived from 6 repeat standard sections. *Prog. Oceanogr.*, **80**, 93–112, <https://doi.org/10.1016/j.pocean.2008.12.003>.
- Østerhus, S., and Coauthors, 2019: Arctic Mediterranean exchanges: A consistent volume budget and trends in transports from two decades of observations. *Ocean Sci.*, **15**, 379–399, <https://doi.org/10.5194/os-15-379-2019>.
- Petrie, B., B. Toulany, and C. Garrett, 1988: The transport of water, heat and salt through the strait of Belle Isle. *Atmos.–Ocean*, **26**, 234–251, <https://doi.org/10.1080/07055900.1988.9649301>.
- Proshutinsky, A., M. Steele, and M.-L. Timmermans, 2016: Forum for Arctic Modeling and Observational Synthesis (FAMOS): Past, current, and future activities. *J. Geophys. Res. Oceans*, **121**, 3803–3819, <https://doi.org/10.1002/2016JC011898>.
- Rahmstorf, S., 2002: Ocean circulation and climate during the past 120,000 years. *Nature*, **419**, 207–214, <https://doi.org/10.1038/nature01090>.
- Reverdin, G., D. Cayan, and Y. Kushnir, 1997: Decadal variability of hydrography in the upper northern North Atlantic in 1948–1990. *J. Geophys. Res.*, **102**, 8505–8531, <https://doi.org/10.1029/96JC03943>.
- Rhein, M., R. Steinfeldt, O. Huhn, J. Sültenfuß, and T. Breckenfelder, 2018: Greenland submarine melt water observed in the Labrador and Irminger Sea. *Geophys. Res. Lett.*, **45**, 10 570–10 578, <https://doi.org/10.1029/2018GL079110>.
- Rodhe, H., 1992: Modeling biogeochemical cycles. *Global Biogeochemical Cycles*. S. S. Butcher et al., Eds., Academic Press, 55–72.
- Schauer, U., and M. Losch, 2019: “Freshwater” in the ocean is not a useful parameter in climate research. *J. Phys. Oceanogr.*, **49**, 2309–2321, <https://doi.org/10.1175/JPO-D-19-0102.1>.
- Schlösser, P., D. Bauch, R. Fairbanks, and G. Bonich, 1994: Arctic river-runoff: Mean residence time on the shelves and in the halocline. *Deep-Sea Res. I*, **41**, 1053–1068, [https://doi.org/10.1016/0967-0637\(94\)90018-3](https://doi.org/10.1016/0967-0637(94)90018-3).
- Schulze Chretien, L. M., and E. Frajka-Williams, 2018: Wind-driven transport of fresh shelf water into the upper 30 m of the Labrador Sea. *Ocean Sci.*, **14**, 1247–1264, <https://doi.org/10.5194/os-14-1247-2018>.
- Schwartz, S. E., 1979: Residence times in reservoirs under non-steady-state conditions: application to atmospheric CO<sub>2</sub> and aerosol sulfate. *Tellus*, **31**, 530–547, <https://doi.org/10.3402/tellusa.v31i6.10471>.
- Sévellec, F., T. Huck, M. B. Jelloul, and J. Vialard, 2009: Nonnormal multidecadal response of the thermohaline circulation induced by optimal surface salinity perturbations. *J. Phys. Oceanogr.*, **39**, 852–872, <https://doi.org/10.1175/2008JPO3998.1>.
- Skogestad, S., 2009: Process dynamics. *Chemical and Energy Process Engineering*, CRC Press, 273–326.
- Stouffer, R. J., 2004: Time scales of climate response. *J. Climate*, **17**, 209–217, [https://doi.org/10.1175/1520-0442\(2004\)017<0209:TSOCR>2.0.CO;2](https://doi.org/10.1175/1520-0442(2004)017<0209:TSOCR>2.0.CO;2).
- , and Coauthors, 2006: Investigating the causes of the response of the thermohaline circulation to past and future climate changes. *J. Climate*, **19**, 1365–1387, <https://doi.org/10.1175/JCLI3689.1>.
- Sutherland, D., and R. Pickart, 2008: The East Greenland Coastal Current: Structure, variability and forcing. *Prog. Oceanogr.*, **78**, 58–77, <https://doi.org/10.1016/j.pocean.2007.09.006>.
- Swingedouw, D., and Coauthors, 2007: Quantifying the AMOC feedbacks during a 2×CO<sub>2</sub> stabilization experiment with land-ice melting. *Climate Dyn.*, **29**, 521–534, <https://doi.org/10.1007/s00382-007-0250-0>.
- , and Coauthors, 2015: On the reduced sensitivity of the Atlantic overturning to Greenland ice sheet melting in projections: A multi-model assessment. *Climate Dyn.*, **44**, 3261–3279, <https://doi.org/10.1007/s00382-014-2270-x>.
- Teschl, G., 2012: *Ordinary Differential Equations and Dynamical Systems*. American Mathematical Society, 356 pp.
- Tesdal, J.-E., R. P. Abernathy, J. I. Goes, A. L. Gordon, and T. W. N. Haine, 2018: Salinity trends within the upper layers of the subpolar North Atlantic. *J. Climate*, **31**, 2675–2698, <https://doi.org/10.1175/JCLI-D-17-0532.1>.
- Trenberth, K. E., and J. T. Fasullo, 2017: Atlantic meridional heat transports computed from balancing Earth's energy locally. *Geophys. Res. Lett.*, **44**, 1919–1927, <https://doi.org/10.1002/2016GL072475>.
- Velicogna, I., and Coauthors, 2020: Continuity of ice sheet mass loss in Greenland and Antarctica from the GRACE and GRACE follow-on missions. *Geophys. Res. Lett.*, **47**, e2020GL087291, <https://doi.org/10.1029/2020GL087291>.
- Weaver, A. J., E. S. Sarachik, and J. Marotzke, 1991: Freshwater flux forcing of decadal and interdecadal oceanic variability. *Nature*, **353**, 836–838, <https://doi.org/10.1038/353836a0>.
- Yashayaev, I., and J. W. Loder, 2016: Recurrent replenishment of Labrador Sea Water and associated decadal-scale variability. *J. Geophys. Res. Oceans*, **121**, 8095–8114, <https://doi.org/10.1002/2016JC012046>.
- , and —, 2017: Further intensification of deep convection in the Labrador Sea in 2016. *Geophys. Res. Lett.*, **44**, 1429–1438, <https://doi.org/10.1002/2016GL071668>.
- , D. Seidov, and E. Demirov, 2015: A new collective view of oceanography of the Arctic and North Atlantic basins. *Prog. Oceanogr.*, **132**, 1–21, <https://doi.org/10.1016/j.pocean.2014.12.012>.